Nano Energy 131 (2024) 110257

Contents lists available at ScienceDirect

Nano Energy

journal homepage: www.elsevier.com/locate/nanoen

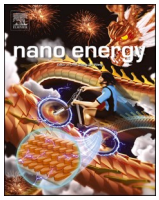

Triboelectric and iontronic dual-responsive bioinspired ionic skin for human–like dexterous robotic manipulation

Dongjie Jiang [a,c,1], Tiantong Wang [a,1], Engui Wang [b,d,1], Jiangtao Xue [b], Wenhao Diao [a], Ming Xu [a], Lin Luo [b,d], Yunbiao Zhao [e], Xiaoting Yuan [a], Jianquan Wang [c], Lecheng Ruan [a], Han Ouyang [b,d,*], Zhou Li [b,d,*], Qining Wang [a,c,f,**]

[a] Department of Advanced Manufacturing and Robotics, College of Engineering, Peking University, Beijing 100871, China
[b] Beijing Institute of Nanoenergy and Nanosystems, Chinese Academy of Sciences, Beijing 101400, China
[c] Peking University Third Hospital, Beijing 100191, China
[d] School of Nanoscience and Engineering, School of Chemical Sciences, University of Chinese Academy of Sciences, Beijing 100049, China
[e] School of Physics, Peking University, Beijing 100871, China
[f] University of Health and Rehabilitation Sciences, Qingdao 266071, China

ARTICLE INFO

Keywords:
Triboelectric nanogenerator
Iontronic
Bioinspired
Dual-responsive
Robotic control

ABSTRACT

Powerful tactile perception is keystone for robots to achieve human-like dexterous manipulation. However, endowing robots with tactile perception capabilities that approach or even surpass those of humans is a challenge. Organisms can perceive complex environments rapidly, and almost all perception is related to the directional transport of ions. Inspired by this mechanism, we design a flexible dual-responsive skin (FDRS) based on ions migration for proximity and tactile somatosensation, which is consisting of single-electrode triboelectric nanogenerator and iontronic sensor, achieving surpassing-skin capabilities. The single-electrode triboelectric nanogenerator can encode the proximity information of approaching targets into a series of voltage pulses with fast response time (100 μs). The iontronic tactile unit based on the hierarchical micro-hemispherical gel layer achieves high linearity ($R^2 = 0.998$) over a broad range of 0–700 kPa. We demonstrate the applications of FDRS for three-dimensional object recognition and robotic control. These capabilities of the multilayer integrated FDRS provide new perspectives for the future development of human-like dexterous robotic manipulation.

1. Introduction

Skin is a multifunctional platform that is critical for the body to communicate with surrounding world. The perception capabilities of skin are originating from its tiny receptors which can convert external stimuli (such as tactile and temperature) into ionic electrical signals available to the brain, enabling the body to response these stimuli in a timely closed-loop process (Fig. 1a-b) [1]. Over the past few decades, the booming era of flexible electronics has promoted the development of bionic ionic skin that can convert external stimuli into directional transport of ions [2,3]. The ultimate goal of developing bionic ionic skin is to emulate, enhance, and expand the functions to natural human skin [4,5]. The emergence bionic ionic skin has demonstrated significant potential in wearable devices, medical electronics, and health monitoring [6–8].

In our interactions with the surroundings, proximity and tactile perception is of great significance [9]. Nevertheless, the tactile sensors on the skin response only when the external stimulus physically contact and unable response to the stimuli prior to contact [10]. Therefore, the human needs a synergy of visual and tactile signals to control the body for better interaction with the external environment (Fig. 1c). However, for artificial sensors, visual signals are usually captured by cameras and tactile signals are provided by pressure sensors [11,12]. Seamless fusion of information between multimodal sensors makes it difficult to respond in a timely manner.

To achieve dual-responsive artificial skin with both proximity and tactile abilities, researchers have conducted extensive exploration [13–15]. Depending on the sensing mechanism, proximity sensing units

* Corresponding authors at: Beijing Institute of Nanoenergy and Nanosystems, Chinese Academy of Sciences, Beijing 101400, China.
** Corresponding author at: Department of Advanced Manufacturing and Robotics, College of Engineering, Peking University, Beijing 100871, China.
E-mail addresses: ouyanghan@binn.cas.cn (H. Ouyang), zli@binn.cas.cn (Z. Li), qiningwang@pku.edu.cn (Q. Wang).
[1] These authors contributed equally.

https://doi.org/10.1016/j.nanoen.2024.110257
Received 30 July 2024; Received in revised form 5 September 2024; Accepted 11 September 2024
Available online 11 September 2024

are usually based on the principles of magnetic field [16,17], electric field [18,19] and humidity [20], while tactile sensing units are usually based on the principles of piezoresistance, capacitance and piezoelectricity [21–23]. Based on the electrostatic induction effect, triboelectric nanogenerator can convert mechanical energy into electrical energy/electrical signals directly without any complicated signal acquisition equipment [24–27]. Triboelectric nanogenerator has been widely used in human–machine interface and wearable electronics, benefit by its many advantages including low cost, simple construction, stable electrical performance, and shape-adaptive ability [28–30]. With the rapid development of machine learning technology, these self-powered sensors provide a new avenue for the realization of embodied intelligence in robotic systems [31,32]. Proximity sensors based on triboelectric nanogenerator have been shown to generate considerable electrical output when approached by naturally charged external targets, and precise distance perception is possible for the system that determine two relatively approaching objects [33,34]. Meanwhile, iontronic sensors are a class of devices with extremely high sensitivity developed in recent years [35]. Different from traditional capacitive pressure sensors, iontronic sensors use an ionic membrane instead of a dielectric layer. Due to the double electric layer (EDL) formed at the electrode/ionic membrane interface, iontronic sensors can achieve high sensitivity and signal enhancement of several orders of magnitude [36]. However, how to integrate proximity and tactile sensors and ultimately achieve a sensory performance beyond the skin, still need to be further explored.

In this study, we report a bioinspired flexible dual-responsive ionic skin (FDRS) with fast response time (100 μs) of proximity interaction and high linearity ($R^2 = 0.998$) over a broad range of 0–700 kPa of tactile interaction. The FDRS based on electrostatic induction and iontronic sensing principles. It allows obtaining two sets of successive non-interfering signals from proximity and tactile interactions. The proximity sensing unit adopts a single-electrode triboelectric nanogenerator (SE-TENG) which comprises a layer of conductive hydrogel acting as the ionic electrode, and an encapsulation of silicone substrate embedded with inorganic electret nanoparticles acting as the electroreceptor. Enable by the electrostatic induction effect, the proximity sensing unit can self-powered convert the proximity information of approaching targets into the voltage pulses signal. The tactile sensing unit utilize iontronic pressure sensor, including two parallel conductive electrodes, a hierarchical micro-hemispherical gel dielectric layer sandwiched in between, and silicone packaging. Upon compression, the micro-hemispherical of different heights were sequentially contacted with the upper electrode. Resulting in a high linearity ($R^2 = 0.998$) over a broad range of 0–700 kPa of the tactile sensing unit. Moreover, we integrated FDRS onto the fingers of robotic hand for intelligent recognition and dexterous grasping of 3D objects through the combination of machine learning which is providing a new perspective for the future development of human-robot interaction flexible electronics.

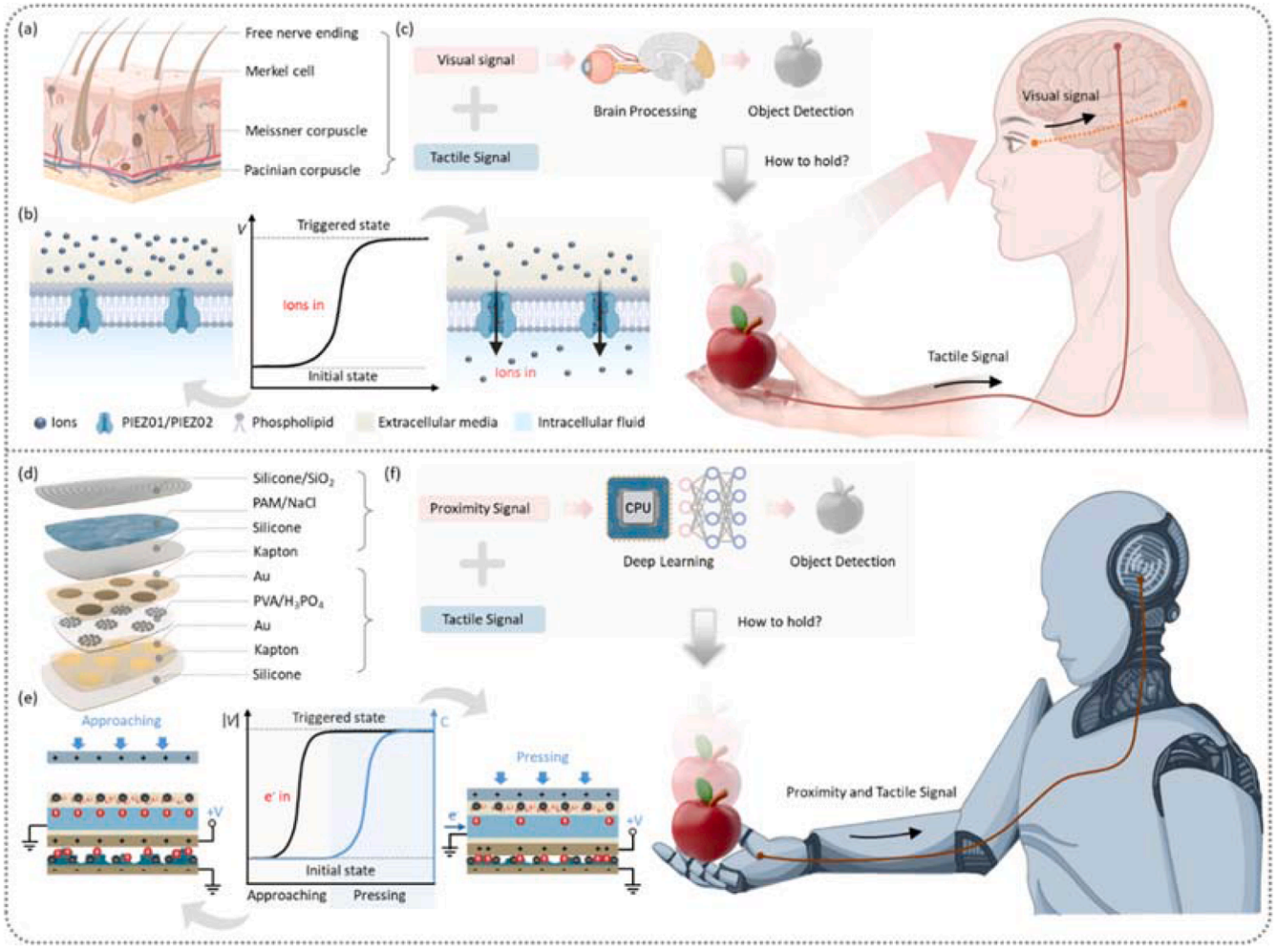

Fig. 1. Bionic principle and structure of flexible bioinspired dual-responsive ionic skin. (a) Illustration of tactile receptors in biological skin. (b) Action potential signal of electrocyte. (c) The process of holding objects in humans requires a synergy of visual and tactile signals. (d) Schematic structure of FDRS. (e) Illustration of the working principle of FDRS. (f) The process of holding objects by the robot with FDRS requires the synergy of proximity and tactile signals. Illustrations in (a) were partially created with BioRender.com.

2. Results and discussion

2.1. Working principle and sensing performance of the proximity unit

Proximity perception is obtained from the single-electrode triboelectric nanogenerator that is based on electrostatic induction. The underlying working principle can be explained using Maxwell's displacement current [37]

$$\varepsilon\nabla \cdot E = \rho - \nabla \cdot P_s \tag{1}$$

$$\nabla \cdot B = 0 \tag{2}$$

$$\nabla \times E = -\frac{\partial B}{\partial t} \tag{3}$$

$$\nabla \times H = J' + \varepsilon\frac{\partial E}{\partial t} + \frac{\partial P_s}{\partial t} \tag{4}$$

$$J_D = \frac{\partial D}{\partial t} = \varepsilon\frac{\partial E}{\partial t} + \frac{\partial P_s}{\partial t} \tag{5}$$

where $\boldsymbol{E}$ is the electric field, $\boldsymbol{B}$ denotes the magnetic field, $\boldsymbol{H}$ stands for magnetizing field intensity, $\boldsymbol{\rho}$ is the free electric charge density, $\boldsymbol{J}$ stands for the free electric current density, $\boldsymbol{t}$ is the time, $\boldsymbol{P_s}$ is the polarization field density, $\boldsymbol{\varepsilon}$ is the permittivity of the dielectrics, and $\boldsymbol{D}$ is the electric displacement field. In Eq. (5), the second component $\frac{\partial P_s}{\partial t}$ in the Maxwell's displacement current is directly related to the output electric current of triboelectric nanogenerator, which enables the potential applications of nanogenerators in energy and sensors [38–40].

The proximity sensing unit can be divided into two parts: elastomeric electret and ionic electrode. The elastomeric electret encapsulation

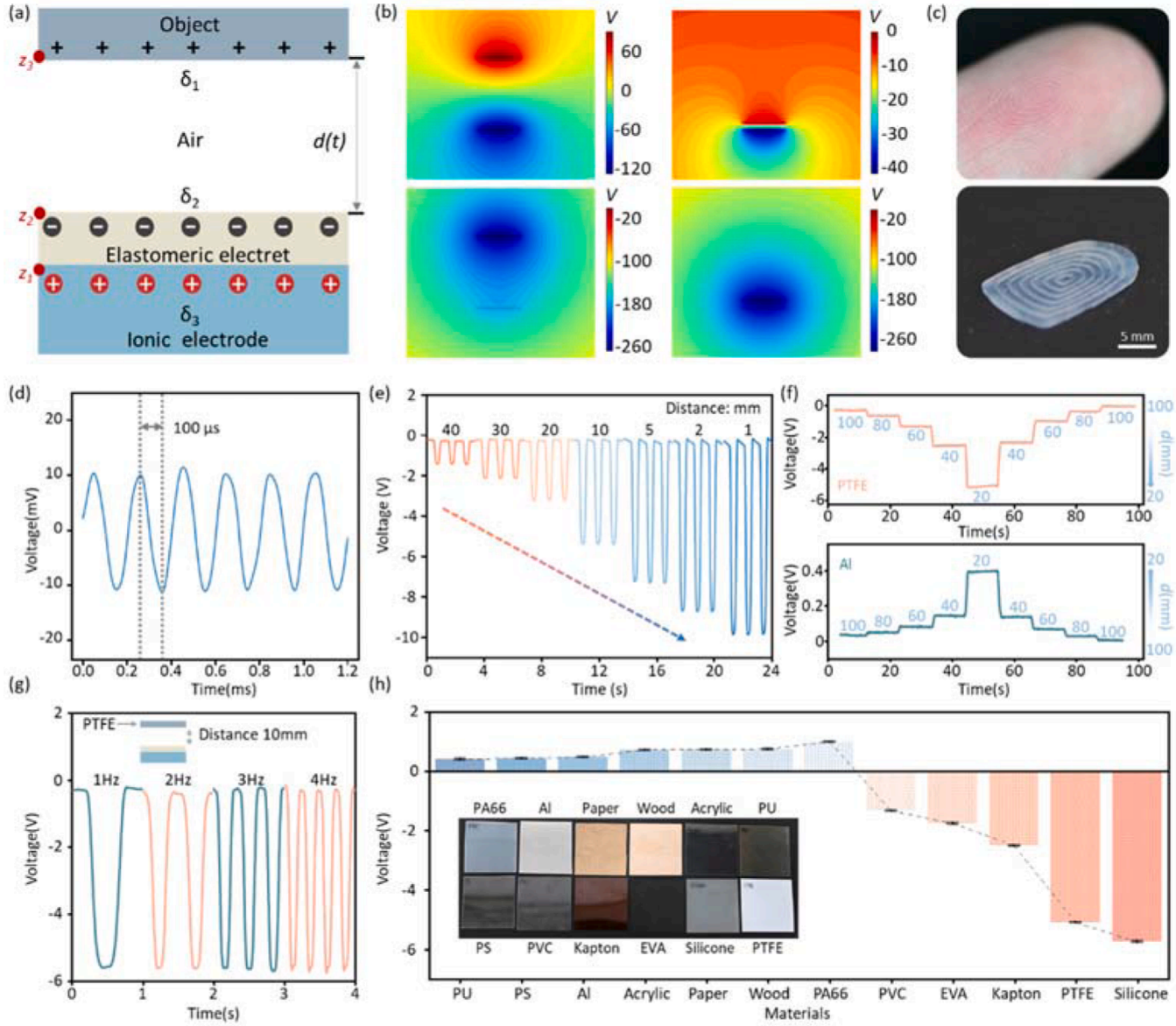

Fig. 2. Working principle and output performance of proximity sensing unit. (a) Schematic diagram of the working mechanism of single-electrode triboelectric nanogenerator. (b) Simulation result of the induced potential when a metal or charged PTFE approach the proximity sensing unit. (c) Elastomeric electret film with fingerprint microstructure. (d) The response time of proximity sensing unit. (e) The relationships between the output voltage of the proximity sensing unit and approaching distance. (f) The real-time output voltage of the proximity sensing unit to the approaching the targets. (g) Output voltage of proximity sensing unit at different proximity frequencies. (h) The applicability of the proximity sensing unit for different materials. All of the approaching objects have a proximity area of 6 cm × 6 cm, and a thickness of 2 mm.

adopts a silicone substrate embedded with inorganic electret nanoparticles (SiO_2), followed by a polarization voltage of 5 kV applied through the corona needle. Therefore, the elastomeric electret is negatively precharged initially. Mixing by SiO_2 nanoparticles can enhance the surface charge density of silicone substrate, and the silicone substrate enables the flexible of the encapsulation. The upper surface of the silicone substrate encapsulation is engineered with microstructures as fingerprints, which can enhance the surface area for electrostatic induction (Fig. 2c). PAM/NaCl conductive hydrogel is selected as the ionic electrode, which ionic conductivity was measured to be 0.566 S/m. The polymerization solution is first injected into the cavity of the elastomeric electret encapsulation and then heated at 50 ℃ for 2 h to polymerize the monomer (Fig. S1).

The working principle of proximity perception is schematically described in Fig. 2a. On the basis of electrostatic induction, the elastomeric electret can convert the approaching information of naturally charged objects into electrical voltage signal directly. Since the elastomeric electret is initially negatively precharged, cations in the conductive hydrogel will gather at the interface to balance the static charge. Meanwhile, the equal amount of anion is migrated to the electrical double layer (EDL) between the metal wire/ionic electrode. As an example, when an object with a naturally net positive surface charge approaches the sensor, the number of cations between the ionic electrode and elastomeric electret interface will decreases due to the Maxwell displacement current, and the number of anions at the EDL between the wire and ionic electrode also decreases by an equal amount. This causes electrons transfer from the ground to the EDL through the external circuit, thereby outputting a voltage pulse (Fig. S2). Similarly, if the object has a net negative surface charge, the entire process will be reversed, and the electrons will transfer from the EDL to the ground. Therefore, proximity sensing of the approaching object can be achieved by measuring the output voltage across the external load. To expound the working principle of the proximity sensing unit, we calculate the induced potential of a metal or charged polytetrafluoroethylene (PTFE) object when approaching to the sensor by utilizing the COMSOL Multiphysics software which is based on finite-element simulation (Fig. 2b).

To evaluate the sensing performance of proximity perception, various conditions are simulated by a linear motor. The result shows that the response time of proximity sensing unit is as fast as 100 μs, ensuring accurate proximity information even with quick approaching (Fig. 2d). The output performance of proximity sensing unit is related to the approach distance and material of target object. When the proximity object approaches the sensor from different positions, the absolute value of open-circuit voltage increases significantly as the distance decreases from 40 mm to 1 mm (Fig. 2e). Therefore, precise distance perception is possible for a certain system consisting of two definite objects. As shown in Fig. 2f, when the charged PTFE or metal is approaching and moving away from the sensor, a continuously voltage signal containing the distance information of target can be obtained in real-time. Moreover, the voltage peaks of the sensor are almost equal when the target is in the same position, whether the object is approaching or moving away. Due to the fast response time of the sensor, the output voltage signal of the sensor remains relatively stable when the object approaches and moves away at different frequencies (Fig. 2g). In particular, the sensor is suitable for the approaching objects with different materials, and even can be used for material identification through the characteristics of the proximity signal (Fig. 2h).

2.2. Working principle and sensing performance of the tactile unit

Tactile perception is obtained by utilizing iontronic pressure sensing technique. The capacitance value of an iontronic sensor depends mainly on EDL capacitance, which can be modeled by the Gouy-Chapman-Stern model. The charge on the surface of the electrode plate will have a strong electrostatic interaction with the ions in the electrolyte at the liquid-solid contact interface, at which the ions with the opposite electrical charge on the surface of the electrode plate are attracted to the surface of the electrode, whereas the ions with the same electrical charge on the surface of the electrode plate are repulsed, resulting in the formation of EDL at the electrolyte-electrode interface. The EDL capacitance can be equivalent to a Helmholtz layer capacitance $\boldsymbol{C_H}$ and a diffusion layer capacitance $\boldsymbol{C_D}$ connected in series. Since both $\boldsymbol{C_H}$ and $\boldsymbol{C_D}$ are related to the contact area A of the electrode with the electrolyte, the EDL capacitance $\boldsymbol{C_{EDL}}$ can be written as [41]:

$$C_{EDL} = \left(\frac{1}{C_H} + \frac{1}{C_D}\right)^{-1} = \eta_A \psi(d, \varepsilon, c, \phi, T)A$$

where $\boldsymbol{\eta_A}$ is the roughness ratio, $\boldsymbol{\psi}$ is a function that is determined by the thickness of Helmholtz layer $\boldsymbol{d}$, the dielectric constant $\boldsymbol{\varepsilon}$, concentrations $\boldsymbol{c}$, surface potential $\boldsymbol{\phi}$, and temperature $\boldsymbol{T}$. $\boldsymbol{A}$ is the contact area between the electrolyte and electrode.

As shown in Fig. 3a, after pressure is applied to the sensor, the microstructure on the upper surface of the ionic film gradually increases the contact area between it and the upper electrode plate, and more EDL capacitors are formed at the contact interface. These EDL capacitors are connected in parallel with each other, which greatly increases the magnitude of the change in the output capacitance value of the sensor. The hierarchical design of the microstructures allows the electrodes to contact microstructures with different stiffnesses under pressure, allowing for great linearity over broad pressure range [7,42]. Fig. 3b depicts the hierarchical structures of the ionic film, which were engineered with height gradient and graded microstructures. To further expound the working principle of iontronic tactile sensing unit with the hierarchical micro-hemispherical gel layer, we use Ansys simulation software to calculate the Von Mises stress between the microstructures and upper electrode plate when the sensor is applied an external pressure (Fig. 2c and Video S1).

Supplementary material related to this article can be found online at doi:10.1016/j.nanoen.2024.110257.

The relationship between the output capacitance and the applied pressure is shown in Fig. 3d. The sensitivity of the pressure sensor is defined as $S = \delta(\Delta C/C_0)/\delta P$, where $\Delta\boldsymbol{C}$ is the change of output capacitance, $\boldsymbol{C_0}$ is the initial capacitance before applying any pressure, $\boldsymbol{P}$ is the exerted pressure value. By leveraging the ionic film with hierarchical micro-hemispherical structure, the tactile unit exhibits a high sensitivity of 7.71 kPa^{-1} over a wide range of pressure (0–700 kPa) with high linearity (R^2=0.998). As presented in Fig. 3e, the tactile unit also shows a rapid response and recovery time of 30.77 ms and 38.46 ms, respectively. The high sensitivity over a broad range of pressure allows for high pressure resolution, as shown in Fig. 3f. Being applied with a reference pressure of 160 kPa, the tactile unit is still capable of detecting the pressure increment of 20 kPa and recover to the initial output value after all the pressure is retrieved. The real-time responses of the tactile unit under dynamic loading and unloading of various pressure values (200 Pa, 600 Pa, 1000 Pa, 1500 Pa, 2500 Pa) are shown in Fig. 3g. The tactile unit also features great durability over 15 days, as shown in Fig. 3h. Under the pressure of ~ 6 kPa, the output capacitance of the device remains stable at day 0 and day 15, respectively. The repeatability of the tactile unit was characterized by loading and unloading the pressure of ~ 6 kPa for over 10,000 s (Fig. 3i), during which the output shows no obvious drift.

2.3. Design of FDRS for fingertip

By integrating proximity and tactile sensing units in multiple-layer method, we have designed and fabricated flexible dual-responsive skin (FDRS). To evaluate the sensing performance of FDRS when interacting with the external object, FDRS is utilized to detect the falling process of a tennis ball. As shown in Fig. 4a and b, the tennis ball is placed directly above the FDRS at a distance about 20 cm in the initial stage, and then begins to fall. The entire descent process can be divided into three

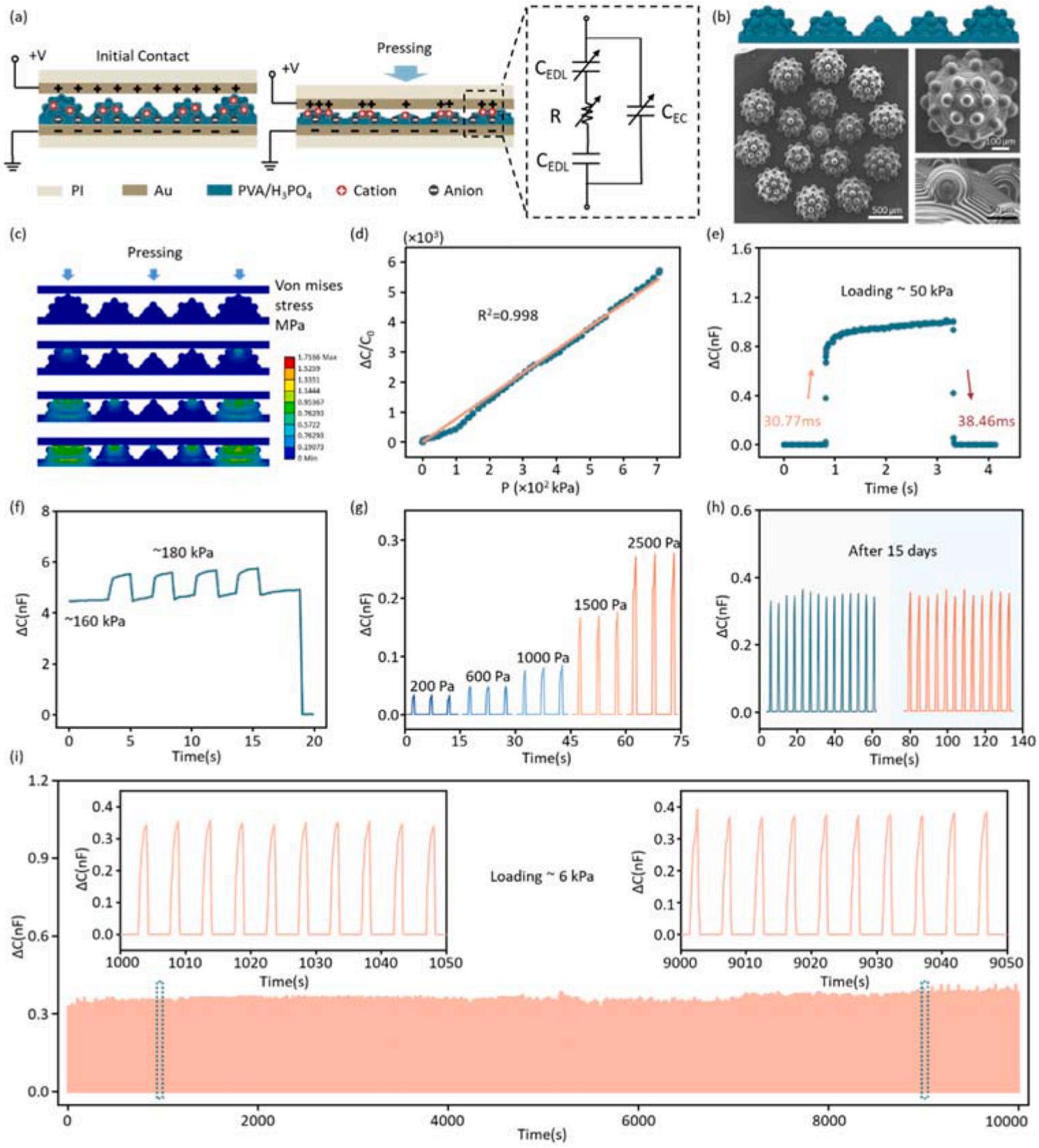

Fig. 3. Working principle and sensing performance of the tactile unit. (a) Schematic illustration of the working principle of the tactile unit based on iontronic sensing before and after exerting pressure. (b) Schematic illustration of cross section of the microstructured ionic film, and the SEM images of ionic film, showing hierarchical structures. (c) Simulation results of stress distribution of the microstructured ionic film under various pressure values. (d) The relationship between normalized output capacitance and the applied pressure. (e) The response time of the tactile unit. (f) The detection of low pressure under high pressure. (g) The repeated output of the tactile unit under dynamic range of pressure. (h) The repeated output of the tactile unit on day 0 and day 15. (i) The stability of the tactile unit tested under the pressure of 6 kPa over 10,000 s.

stages, and the proximity and tactile signals enabled by the FDRS is recorded during the process. In the first stage, the distance between the tennis ball and FDRS is beyond the detection range, so the proximity signal of the FDRS has not changed. As the tennis ball drops rapidly into the FDRS detection range, the ΔU of the proximity signal decreases from 0 V to −5.4 V and the tactile signal ΔC nearly remains stable. However, when the tennis ball is about to touch the FDRS, there is a tiny fluctuation of ΔC, which is due to the presence of self-capacitance in the iontronic tactile sensor. The application of an exciting signal to the electrode induces a changing electric field between the electrode and the

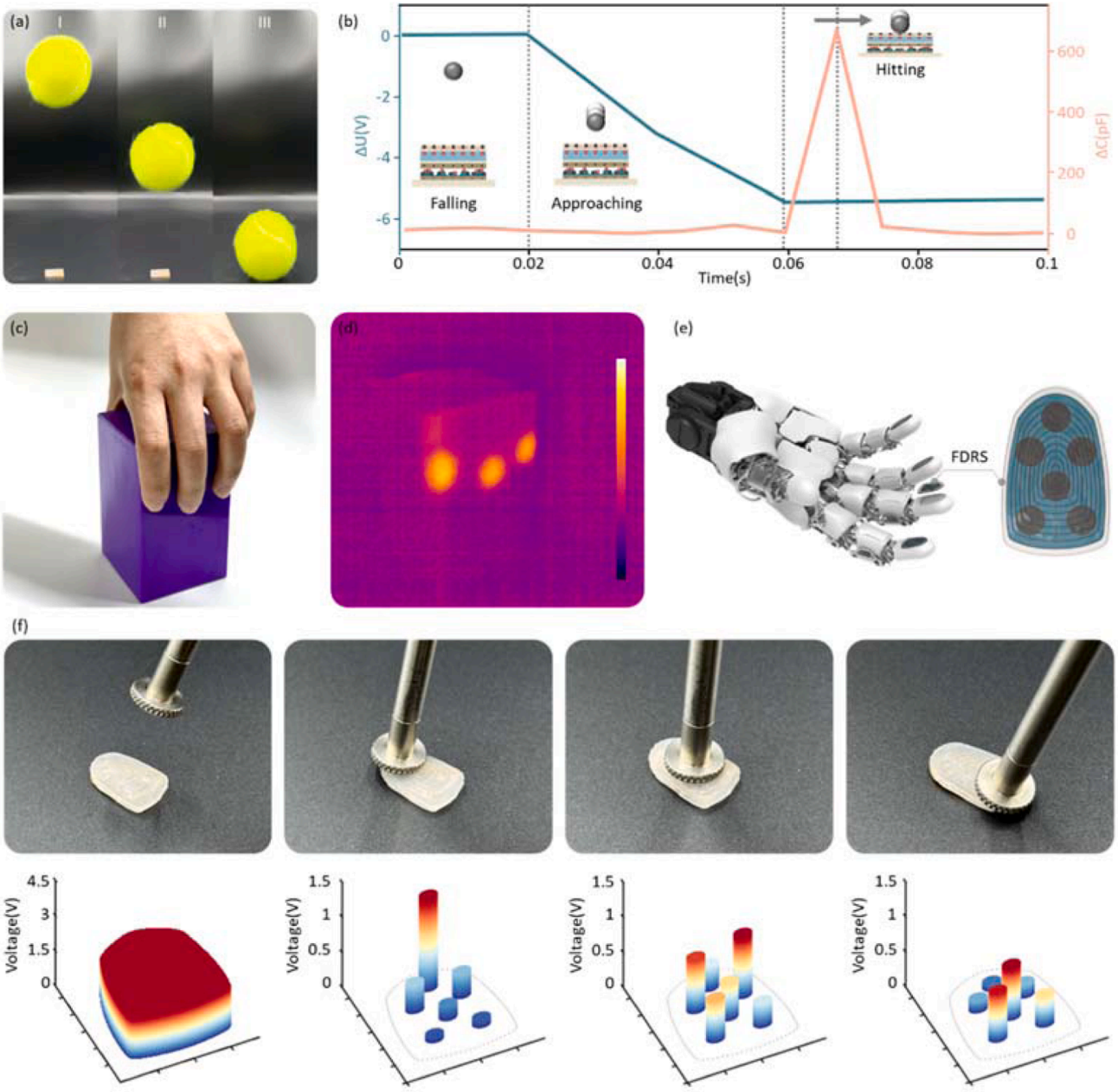

Fig. 4. Characterization results of FDRS and the design of fingertip-shaped sensor. (a) Images and (b) sensing signals of FDRS when a tennis ball is dropping on it (Distance: ~20 cm). (c) Photograph of a hand grasping a rectangle and (d) the thermography image after a period of grasping time. (e) The design of fingertip-shaped sensor with 6 tactile sensing pixels and a large proximity sensing unit. (f) Output signals of FDRS when approaching and pressing different pixels with a metal rod.

ground. Therefore, the parasitic capacitance between the tennis ball and the ground will also change when is about to contact the FDRS. In the final stage, the tennis ball contact with the FDRS and the tactile signal ΔC increases to ~660 pF dramatically. In particular, since the size of a single tactile sensing unit is a circle with a diameter of 3 mm and the size of the proximity sensing unit is 10 mm × 20 mm in this test, the proximity signal ΔU remains stable when the tactile signal ΔC reverts to initial value, because the tennis ball remains in contacting with the proximity sensing unit.

The thermogram reveals that when the human hand is grasping the object, it mainly relies on the fingertips for operation (Fig. 4c, d). To equip the robotic hand with the FDRS, we design and fabricate the FDRS into a fingertip shaped. As shown in Fig. 4e, each FDRS fingertip sensor contains 6 tactile sensing pixels and a large proximity sensing unit. A customized capacitance-to-voltage circuit is employed to acquire the output signals of the tactile sensing array. Here, a metal rod is used to approach and press the FDRS. When the metal rod is approach to the FDRS fingertip sensor, the voltage signal of the proximity sensing unit increases rapidly. And when the metal rod is loaded at different pixels of the array, the tactile sensing unit can show significant pressure changes and differences of pressure distribution (Fig. 4f). Arrayed 6 pixels improve the spatial resolution of tactile sensing.

2.4. *Machine learning–aided dual-responsive somatosensation robotic hand*

To further explore and extend the application scenarios of FDRS, five fingertip-shaped FDRS sensors as shown in Fig. 4e, f are integrated onto the robotic hand (Fig. 5a). Because the targets with different 3D shapes have particular spatial distances to each finger when they approach to

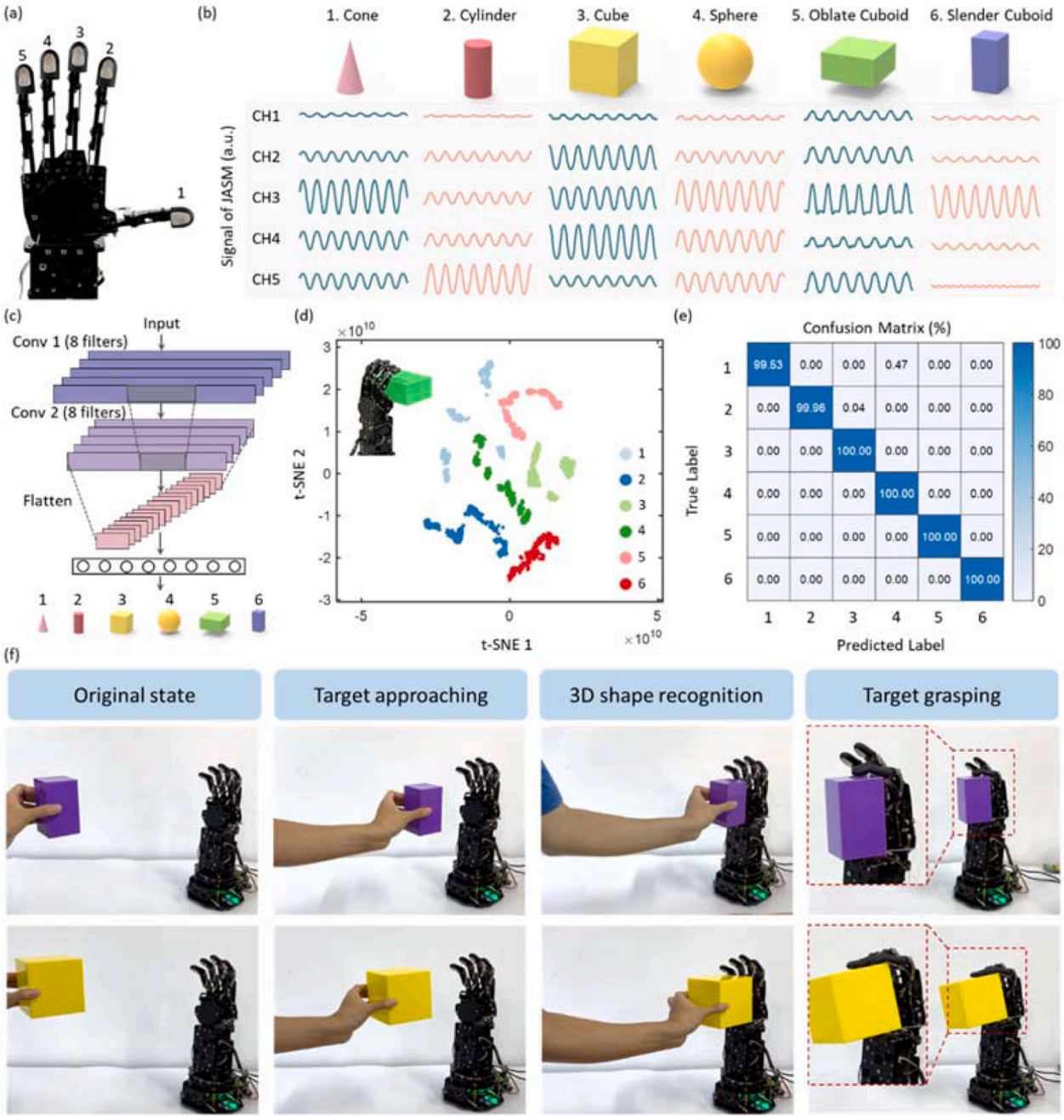

Fig. 5. Machine learning–aided dual-responsive somatosensation robotic hand. (a) The FDRS-based robotic hand. (b) The proximity sensing signals of the 5 channels when the different 3D shape objects periodically approaching and moving away from the robotic hand. (c) Architecture of 1D-CNN that is used for precontact object recognition. (d) t-SNE visualization of the clustered features of different objects. (e) Confusion matrix for classifying 6 objects. (f)The FDRS-based robotic hand intelligently use 5 fingers to grab the cube and switch to use 3 fingers to grab the slender cuboid.

the robotic hand, the proximity sensor signals of each FDRS have unique characteristics in the meantime. We first explore the ability of FDRS to recognize objects with different 3D shapes. The targets are simulated by a linear motor for reciprocating linear motion to periodically approaching and moving away from the robotic hand. The electrical output voltage signals of proximity sensing unit are captured by five electrometers and recorded by an oscilloscope (Video S2). To observation and comparison convenient, the proximity sensing signals of the 5 channels are normalized as a composite data set and expressed in amplitude. The amplitude is proportional to the output voltage value of the FDRS. As shown in Fig. 5b, the proximity sensing signals of the 5 channels are significantly different, and the signal characteristics are various from the targets of different 3D shapes.

Supplementary material related to this article can be found online at doi:10.1016/j.nanoen.2024.110257.

The collected data of each sensing channel is segmented into approaching phase (when the targeted target approaches the robotic hand) and departing phase (when the target departs the robotic hand). A sliding window with the length of 250 ms and the step size of 50 ms was applied to each approaching phase of each channel, then the acquired dataset was batch-normalized and fed into the feature extraction network. A one-dimensional convolutional neural network (1D-CNN) was employed to extract temporal features of the waveforms of the multi-channel proximity units and classify into different object

categories. The architecture of the designed 1D-CNN is shown in Fig. 5c, which contains 2 convolutional layers (each contains 8 filters with the kernel size of 3×1 and activated by ReLU function), followed by a flatten layer. The flatten layer is fully connected to a dense layer with 8 neurons, then the output is connected to the output layer, which is activated with the softmax function. 10-fold cross validation was used to validate the recognition performance, and the network was trained with cross-entropy loss over 20 epochs. After the feature extraction, the data was visualized in a lower dimension using t-distributed stochastic neighbor embedding (t-SNE) [43], as shown in Fig. 5d. The clustered sample points indicated excellent distinction among different object types. Over 10 rounds of validation, the 1D-CNN achieved an average classification accuracy of 99.92 %, and the confusion matrix is presented in Fig. 5e. Thus, the machine learning–aided robotic hand with FDRS for 3D object shape recognition is proved to be feasible.

Furthermore, we demonstrate the FDRS-based robotic hand for real-time grasping of objects with different 3D shapes. The proximity and tactile signals of five robotic fingers were simultaneously collected by the signal acquisition system (Fig. S5). In general, machine learning algorithms with more accuracy usually require higher computational power, although they can provide more delicate recognition of different targets. However, in this case, it is more difficult to realize real-time feedback control of the robot. Here, we realize the real-time recognition for different shapes objects and feedback grasping with particular gestures of the robotic hand by amplitude threshold judgment of multi-channel sensor signals. Due to the limitations of the hardware system, including the signals transmission module delay and the requirements of the data analysis module, the program processes the data every 3 ms. The FDRS-based robotic hand can recognizes cube and slender cuboid, and feedback grasping with particular gestures in real time. As shown in Fig. 5f and Video S3, the FDRS-based robotic hand can intelligently use 5 fingers to grab the cube and switch to use 3 fingers to grab the slender cuboid, respectively.

Supplementary material related to this article can be found online at doi:10.1016/j.nanoen.2024.110257.

3. Conclusions

Human-robot system is evolving towards intelligence and dexterity, which requires multimodal sensing information. In this work, we proposed a bioinspired flexible dual-responsive skin (FDRS) based on ions migration for proximity and tactile somatosensation, which can realize a fast response time (100 μs) of proximity interaction and high linearity ($R^2 = 0.998$) over a broad range of 0–700 kPa of tactile interaction. The FDRS is based on Maxwell displacement current to detect the charge naturally carried by the target, and it is capable to convert the proximity information of object directly into a voltage pulse signal. A wide variety of material types can be detected by FDRS, including natural material, metal and polymer. The linearity of FDRS for tactile sensing is improved by designing and fabricating the hierarchical micro-hemispherical gel layer. Machine learning-aided dual-responsive somatosensation robotic hand was then developed to demonstrate the feasibility of including sensing approaching targets, 3D objects shape recognition and intelligent visionless grasping by the robotic hand. It is expected that this kind of dual-responsive ionic skin will have great potential in the fields of human-robot interactions.

4. Experimental section

4.1. Preparation of elastomeric electret

First, 2 wt% SiO_2 nanoparticles (Specific surface area: 400 m^2/g) was added to Ecoflex 00–30 and thoroughly stirred by planetary gravity mixer for 1 min. Then the mixture was dripped onto the PTFE mold and vacuumed to fully defoam. and cured at ambient temperature (70 ℃) for 2 h. Finally, put the demolded film on the Cu bottom electrode, and a polarization voltage of 5 kV is applied through the corona needle for 15 minutes.

4.2. Preparation of PVA/H_3PO_4 ionic film with the hierarchical micro-hemispherical structure

First, 4 g of PVA (Mw: 145,000) was added to 36 g of deionized water and thoroughly stirred at 90 ℃ for 2 h. When the solution was cooled to 50 ℃, 3.2 mL of H_3PO_4 (AR, ≥85 %) was added and stirred at 50 ℃ for another 2 h. After complete mixture, the ionic precursor was dripped onto the mold with 3D-printed microstructures, vacuumed to fully defoam, and cured at ambient temperature (25 ℃) for 24 h. The PVA/H_3PO_4 ionic film with the thickness of 300 μm was peeled off from the mold and cut into circles (diameter: 3 mm) for later use.

4.3. Preparation of PAM/NaCl conductive hydrogel

Acrylamide monomer (30 wt%) and NaCl (4 M) powder were dissolved in deionized water. Then, N, N′-methylenebisacrylamide (0.05 wt %), ammonium persulphate (0.17 wt%) and N, N, N′, N′-tetramethylethylenediamine (0.05 wt%) were subsequently added into the mixture above. The uniformly mixed solution was transferred into silicone mold by the syringe and then gelled in an oven at 50 °C for 2 h.

4.4. Characterization and measurements

The proximity sensing unit (single-electrode triboelectric nanogenerator) is simulated by a linear motor for various motion conditions. The electrical output voltage signals of proximity sensing unit are captured by electrometers (Keithley 6518) and recorded by an oscilloscope (HDO 8108 A, Teledyne LeCroy). The surface morphology of hierarchical micro-hemispherical gel layer is measured using a scanning electron microscope (S-4800, Hitachi). The interfacial capacitance of tactile sensing unit for various motion conditions are measured by using an LCR meter (E4980AL, Keysight), and simulated by a vertically mechanical test platform (ESM303, Mark-10) equipped with a force gauge (M5–5, Mark-10). The response time of tactile sensing unit is measured by a super-fast LCR meter (TH2840A, Tonghui). The output signal of the tactile sensing array is collected by a customized capacitance-to-voltage circuit.

CRediT authorship contribution statement

Jianquan Wang: Supervision. **Xiaoting Yuan:** Visualization, Investigation. **Yunbiao Zhao:** Supervision. **Lin Luo:** Investigation, Data curation. **Engui Wang:** Methodology, Data curation. **Zhou Li:** Writing – review & editing, Supervision, Project administration, Methodology, Funding acquisition. **Tiantong Wang:** Writing – original draft, Visualization, Methodology, Data curation. **Han Ouyang:** Writing – original draft, Methodology, Funding acquisition, Conceptualization. **Dongjie Jiang:** Writing – original draft, Visualization, Methodology, Investigation, Data curation, Conceptualization. **Lecheng Ruan:** Software. **Qining Wang:** Writing – review & editing, Supervision, Project administration, Methodology, Funding acquisition. **Ming Xu:** Formal analysis. **Wenhao Diao:** Validation. **Jiangtao Xue:** Visualization, Software.

Declaration of Competing Interest

The authors declare that they have no known competing financial interests or personal relationships that could have appeared to influence the work reported in this paper.

Data availability

Data will be made available on request.

Acknowledgements

This work was supported by the National Natural Science Foundation of China (Grant Nos. 91948302, 52373256, T2125003), Youth Innovation Promotion Association CAS (Grant No. 2023176), China Postdoctoral Science Foundation (Grant No. 2023M740100), Beijing Natural Science Foundation (L212010, L245015, Z240022), The Fundamental Research Funds for the Central Universities.

Appendix A. Supporting information

Supplementary data associated with this article can be found in the online version at doi:10.1016/j.nanoen.2024.110257.

References

[1] A. Zimmerman, L. Bai, D.D. Ginty, The gentle touch receptors of mammalian skin, Science 346 (2014) 950–954, https://doi.org/10.1126/science.1254229.
[2] J.Y. Sun, C. Keplinger, G.M. Whitesides, Z.G. Suo, Ionic skin, Adv. Mater. 26 (2014) 7608–7614, https://doi.org/10.1002/adma.201403441.
[3] M. Wang, Y.F. Luo, T. Wang, C.J. Wan, L. Pan, S.W. Pan, K. He, A. Neo, X.D. Chen, Artificial skin perception, Adv. Mater. 33 (2021) e2003014, https://doi.org/10.1002/adma.202003014.
[4] Y. Dobashi, D. Yao, Y. Petel, T.N. Nguyen, M.S. Sarwar, Y. Thabet, C.L.W. Ng, E. S. Glitz, G.T.M. Nguyen, C. Plesse, F. Vidal, C.A. Michal, J.D.W. Madden, Piezoionic mechanoreceptors: force-induced current generation in hydrogels, Science 376 (2022) 502–507, https://doi.org/10.1126/science.aaw1974.
[5] Q.N. Zhuang, K.M. Yao, C. Zhang, X. Song, J.K. Zhou, Y.F. Zhang, Q.Y. Huang, Y. Z. Zhou, X.G. Yu, Z.J. Zheng, Permeable, three-dimensional integrated electronic skins with stretchable hybrid liquid metal solders, Nat. Electron. (2024) 1–12, https://doi.org/10.1038/s41928-024-01189-x.
[6] Z.P. Feng, Q. He, J. Qiu, X. Wang, Y.G. Lin, Y.F. Wu, J. Yang, Iontronic textile-based capacitive pressure sensor for unconstrained respiration and heartbeat monitoring, Adv. Mater. Technol.. 8 (2023) 2300949, https://doi.org/10.1002/admt.202300949.
[7] R.X. Yang, A. Dutta, B.W. Li, N. Tiwari, W.Q. Zhang, Z.Y. Niu, Y.Y. Gao, D. Erdely, X. Xin, T.J. Li, H.Y. Cheng, Iontronic pressure sensor with high sensitivity over ultra-broad linear range enabled by laser-induced gradient micro-pyramids, Nat. Commun. 14 (2023) 2907, https://doi.org/10.1038/s41467-023-38274-2.
[8] Y. Zou, P.C. Tan, B.J. Shi, H. Ouyang, D.J. Jiang, Z. Liu, H. Li, M. Yu, C. Wang, X. C. Qu, L.M. Zhao, Y.B. Fan, Z.L. Wang, Z. Li, A bionic stretchable nanogenerator for underwater sensing and energy harvesting, Nat. Commun. 10 (2019) 2695, https://doi.org/10.1038/s41467-019-10433-4.
[9] Z.H. Guo, H.L. Wang, J.J. Shao, Y.S. Shao, L.Y. Jia, L.W. Li, X. Pu, Z.L. Wang, Bioinspired soft electroreceptors for artificial precontact somatosensation, Sci. Adv. 8 (2022) eabo5201, https://doi.org/10.1126/sciadv.abo5201.
[10] M.L. Zhu, Z.D. Sun, Z.X. Zhang, Q.F. Shi, T.Y.Y. He, H.C. Liu, T. Chen, C.K. Lee, Haptic-feedback smart glove as a creative human-machine interface (HMI) for virtual/augmented reality applications, Sci. Adv. 6 (2020) eaaz8693, https://doi.org/10.1126/sciadv.aaz8693.
[11] C. Bartolozzi, L. Natale, F. Nori, G. Metta, Robots with a sense of touch, Nat. Mater. 15 (2016) 921–925, https://doi.org/10.1038/nmat4731.
[12] Y. Cao, Y. Yang, X.C. Qu, B.J. Shi, L.L. Xu, J.T. Xue, C. Wang, Y. Bai, Y.S. Gai, D. Luo, Z. Li, A self-powered triboelectric hybrid coder for human-machine interaction, Small Methods 6 (2022) e2101529, https://doi.org/10.1002/smtd.202101529.
[13] S.C. Chen, Y.F. Wang, L. Yang, Y.J. Guo, M. Wang, K. Sun, Flexible and transparent sensors with hierarchically micro-nano texture for touchless sensing and controlling, Nano Energy 82 (2021) 105719, https://doi.org/10.1016/j.nanoen.2020.105719.
[14] W.B. Liu, Y.N. Duo, J.Q. Liu, F.Y. Yuan, L. Li, L.C. Li, G. Wang, B.H. Chen, S. Q. Wang, H. Yang, Y.C. Liu, Y.R. Mo, Y. Wang, B. Fang, F.C. Sun, X.L. Ding, C. Zhang, L. Wen, Touchless interactive teaching of soft robots through flexible bimodal sensory interfaces, Nat. Commun. 13 (2022) 5030, https://doi.org/10.1038/s41467-022-32702-5.
[15] W.J. Liu, F.H. Xiang, D.Q. Mei, Y.C. Wang, A flexible dual-mode capacitive sensor for highly sensitive touchless and tactile sensing in human-machine interactions, Adv. Mater. Technol. 9 (2024) 2301685, https://doi.org/10.1002/admt.202301685.
[16] J. Ge, X. Wang, M. Drack, O. Volkov, M. Liang, G.S.C. Bermúdez, R. Illing, C. A. Wang, S.Q. Zhou, J. Fassbender, M. Kaltenbrunner, D. Makarov, A bimodal soft electronic skin for tactile and touchless interaction in real time, Nat. Commun. 10 (2019) 4405, https://doi.org/10.1038/s41467-019-12303-5.
[17] W.B. Liu, Y. Duo, X.Y. Chen, B.H. Chen, T.Z. Bu, L. Li, J.X. Duan, Z.H. Zuo, Y. Wang, B. Fang, F.C. Sun, K. Xu, X.L. Ding, C. Zhang, L. Wen, An intelligent robotic system capable of sensing and describing objects based on bimodal, self-powered flexible sensors, Adv. Funct. Mater. 33 (2023) 2306368, https://doi.org/10.1002/adfm.202306368.
[18] H.C. Guo, Y.J. Tan, G. Chen, Z.F. Wang, G.J. Susanto, H.H. See, Z.J. Yang, Z. W. Lim, L. Yang, B.C.K. Tee, Artificially innervated self-healing foams as synthetic piezo-impedance sensor skins, Nat. Commun. 11 (2020) 5747, https://doi.org/10.1038/s41467-020-19531-0.
[19] M.S. Sarwar, Y. Dobashi, C. Preston, J.K.M. Wyss, S. Mirabbasi, J.D.W. Madden, Bend, stretch, and touch: Locating a finger on an actively deformed transparent sensor array, Sci. Adv. 3 (2017) e1602200, https://doi.org/10.1126/sciadv.1602200.
[20] S.S. Ding, X. Jin, B. Wang, Z.H. Niu, J.Y. Ma, X.M. Zhao, M.J. Yang, C.C. Wang, Q. Shi, X.Y. Li, Integrating $Ti_3C_2T_x$ MXene nanosheets with thermoplastic polyurethane nanofibers as wearable humidity sensors for noninvasive sleep monitoring and noncontact sensing, ACS Appl. Nano Mater. 6 (2023) 11810–11821, https://doi.org/10.1021/acsanm.3c01732.
[21] X.C. Qu, Z. Liu, P.C. Tan, C. Wang, Y. Liu, H.Q. Feng, D. Luo, Z. Li, Z.L. Wang, Artificial tactile perception smart finger for material identification based on triboelectric sensing, Sci. Adv. 8 (2022) eabq2521, https://doi.org/10.1126/sciadv.abq2521.
[22] T. Jin, Z.D. Sun, L. Li, Q. Zhang, M.L. Zhu, Z.X. Zhang, G.J. Yuan, T. Chen, Y. Z. Tian, X.Y. Hou, C. Lee, Triboelectric nanogenerator sensors for soft robotics aiming at digital twin applications, Nat. Commun. 11 (2020) 5381, https://doi.org/10.1038/s41467-020-19059-3.
[23] H.L. Jia, Y.Y. Gao, J.K. Zhou, J. Li, C.K. Yiu, W. Park, Z.H. Yang, X.E. Yu, A deep learning-assisted skin-integrated pulse sensing system for reliable pulse monitoring and cardiac function assessment, Nano Energy 127 (2024) 109796, https://doi.org/10.1016/j.nanoen.2024.109796.
[24] H.Y. Guo, X.J. Pu, J. Chen, Y. Meng, M.H. Yeh, G.L. Liu, Q. Tang, B.D. Chen, D. Liu, S. Qi, C.S. Wu, C.G. Hu, J. Wang, Z.L. Wang, A highly sensitive, self-powered triboelectric auditory sensor for social robotics and hearing aids, Sci. Robot. 3 (2018) eaat2516, https://doi.org/10.1126/scirobotics.aat2516.
[25] X.J. Pu, H.Y. Guo, J. Chen, X. Wang, Y. Xi, C.G. Hu, Z.L. Wang, Eye motion triggered self-powered mechnosensational communication system using triboelectric nanogenerator, Sci. Adv. 3 (2017) e1700694, https://doi.org/10.1126/sciadv.1700694.
[26] F. Wen, Z.X. Zhang, T.Y. He, C.K. Lee, AI enabled sign language recognition and VR space bidirectional communication using triboelectric smart glove, Nat. Commun. 12 (2021) 5378, https://doi.org/10.1038/s41467-021-25637-w.
[27] H. Zheng, L.Y. Li, M.H. Haider, D.L. Wen, P.P. Zhi, C. Tu, X.G. Ma, J. Xu, Z.L. Wang, X.S. Zhang, Nanogenerators integrated self-powered multi-functional wings for biomimetic micro flying robots, Nano Energy 101 (2022) 107627, https://doi.org/10.1016/j.nanoen.2022.107627.
[28] X. Li, J. Luo, K. Han, X. Shi, Z. Ren, Y. Xi, Y. Ying, J. Ping, Z.L. Wang, Stimulation of ambient energy generated electric field on crop plant growth, Nat. Food 3 (2022) 133–142, https://doi.org/10.1038/s43016-021-00449-9.
[29] J. Luo, W. Gao, Z.L. Wang, The triboelectric nanogenerator as an innovative technology toward intelligent sports, Adv. Mater. 33 (2021) 2004178, https://doi.org/10.1002/adma.202004178.
[30] T. Chen, Q. Shi, M. Zhu, T. He, L. Sun, L. Yang, C. Lee, Triboelectric self-powered wearable flexible patch as 3D motion control interface for robotic manipulator, ACS Nano 12 (2018) 11561–11571, https://doi.org/10.1021/acsnano.8b06747.
[31] P. Fang, Ml Zhu, Zb Zeng, Wx Lu, F.X. Wang, L. Zhang, T. Chen, Ln Sun, A multi-module sensing and bi-directional HMI integrating interaction, recognition, and feedback for intelligent robots, Adv. Funct. Mater. 34 (2024) 2310254.
[32] M. Zhu, Z. Sun, Z. Zhang, Q. Shi, T. He, H. Liu, T. Chen, C. Lee, Haptic-feedback smart glove as a creative human-machine interface (HMI) for virtual/augmented reality applications, Sci. Adv. 6 (2020) eaaz8693, https://doi.org/10.1126/sciadv.aaz8693.
[33] G.M. Ye, Q. Wu, Y. Chen, X.K. Wang, Z.M. Xiang, J.Y. Duan, Y.F. Wan, P. Yang, Bimodal coupling haptic perceptron for accurate contactless gesture perception and material identification, Adv. Fiber Mater. (2024) 1–13, https://doi.org/10.1007/s42765-024-00458-w.
[34] X.C. Qu, J.T. Xue, Y. Liu, W. Rao, Z. Liu, Z. Li, Fingerprint-shaped triboelectric tactile sensor, Nano Energy 98 (2022) 107324, https://doi.org/10.1016/j.nanoen.2022.107324.
[35] N.N. Bai, Y.H. Xue, S.Q. Chen, L. Shi, J.L. Shi, Y. Zhang, X.Y. Hou, Y. Cheng, K. X. Huang, W.D. Wang, J. Zhang, Y. Liu, C.F. Guo, A robotic sensory system with high spatiotemporal resolution for texture recognition, Nat. Commun. 14 (2023) 7121, https://doi.org/10.1038/s41467-023-42722-4.
[36] Y.F. He, Y. Cheng, C.H. Yang, C.F. Guo, Creep-free polyelectrolyte elastomer for drift-free iontronic sensing, Nat. Mater. (2024) 1–8, https://doi.org/10.1038/s41563-024-01848-6.
[37] Z.L. Wang, On Maxwell's displacement current for energy and sensors: the origin of nanogenerators, Mater. Today 20 (2017) 74–82, https://doi.org/10.1016/j.mattod.2016.12.001.
[38] M.L. Zhu, Z.D. Sun, T. Chen, C.K. Lee, Low cost exoskeleton manipulator using bidirectional triboelectric sensors enhanced multiple degree of freedom sensory system, Nat. Commun. 12 (2021) 2692, https://doi.org/10.1038/s41467-021-23020-3.
[39] G. Yao, L. Kang, C.C. Li, S.H. Chen, Q. Wang, J.Z. Yang, Y. Long, J. Li, K.N. Zhao, W.N. Xu, W.B. Cai, Y. Lin, X.D. Wang, A self-powered implantable and bioresorbable electrostimulation device for biofeedback bone fracture healing, Proc. Natl. Acad. Sci. USA 118 (2021) e2100772118, https://doi.org/10.1073/pnas.2100772118.
[40] X.C. Qu, S.J. Cheng, Y. Liu, Y.R. Hu, Y.Z. Shan, R.Z. Luo, S.X. Weng, H. Li, H.X. Niu, M. Gu, Y.B. Fan, B.J. Shi, Z. Liu, W. Hua, Z. Li, Z.L. Wang, Bias-free cardiac monitoring capsule, Adv. Mater. (2024) 2402457, https://doi.org/10.1002/adma.202402457.

[41] Y. Chang, L. Wang, R.Y. Li, Z.C. Zhang, Q. Wang, J.L. Yang, C.F. Guo, T.R. Pan, First decade of interfacial iontronic sensing: from droplet sensors to artificial skins, Adv. Mater. 33 (2021) 2003464, https://doi.org/10.1002/adma.202003464.
[42] S.W. Wu, C.X. Yang, J.F. Hu, M.C. Pan, W.Z. Meng, Y. Liu, P.S. Li, J.P. Peng, Q. Zhang, P.T. Chen, H.M. Wang, Normal-direction graded hemispheres for ionic flexible sensors with a record-high linearity in a wide working range, ACS Appl. Mater. Interfaces 15 (2023) 47733, https://doi.org/10.1021/acsami.3c09580.
[43] L. van der Maaten, G. Hinton, Visualizing data using t-SNE, J. Mach. Learn. Res. 9 (2008) 2579–2605.

Dongjie Jiang received his Ph.D. in Biophysics from University of Chinese Academy of Sciences in 2022. Currently, he is a postdoctoral fellow at College of Engineering, Peking University. His research interests are focusing on self-powered biomedical systems, in vivo energy harvesters and biosensors.

Tiantong Wang received her Ph.D. in General Mechanics and Foundation of Mechanics from Peking University in 2024. Currently, she is a postdoctoral fellow at School of Mechatronical Engineering, Beijing Institute of Technology. Her research interests are focusing on human-machine interfaces and robotic tactile sensing.

Engui Wang received his master degree from Guangxi University in 2022. Now, He is currently studying for a doctor degree as a joint student under the supervision of Professor Zhou Li and Ouyang Han at the University of Chinese Academy of Sciences. His research focuses on Biodegradable energy devices.

Jiangtao Xue received his Bachelor's degree from Beijing Institute of Technology in 2016. He is currently a Ph.D. student at the Institute of Engineering Medicine, Beijing Institute of Technology. His research interests mainly focus on nanogenerators and wearable electronics.

Wenhao Diao received his B.Eng. in Mechanical and Electronic Engineering from Beijing Institute of Technology in 2024. Currently, he is a research assistant at College of Engineering, Peking University. His research interests are focusing on biosensors.

Ming Xu received the M.E. degree in mechanical engineering in 2023 from Peking University, Beijing, China, where he is currently working toward the Ph.D. degree in dynamics and control with the College of Engineering. His research interests include wearable robotics, exoskeletons, and human–robot interaction.

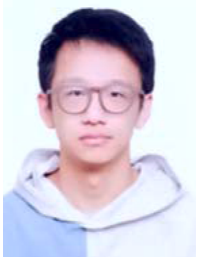

Lin Luo received his Bachelor's Degree from Harbin Normal University in 2021 Currently, he is currently a PhD student in the School of Chemical Science and Engineering at the University of Chinese Academy of Sciences. His research interests are focusing on Implantable wireless electrical stimulator.

Yunbiao Zhao received his Ph.D degree from Peking University in 2020. Currently, he is a research associate professor in school of physics, Peking University. His research interests cover a wide range of topics, including ion beam for nanomaterials, advanced radiation detection and robotic tactile sensing system.

Xiaoting Yuan received her Ph.D. degree in Materials Science and Engineering from Peking University, China, in 2022. Currently she is an engineer at Peking University, China. Her research focuses on 3D-printing prepared flexible piezoelectric electronics.

Prof. Jianquan Wang, the director of the Department of Sports Medicine, Peking University Third Hospital. He has been elected as the new Chairman of the Chinese Society of Sports Medicine in 2023, which is the leading organization for sports medicine in China. He is dedicated to the development of sports medicine and arthroscopy technology, especially in the research and development of new technologies based on biomaterials.

Lecheng Ruan received the B.S. honor degree in Robotics from Harbin Institute of Technology in 2015, and the Ph.D. degree in system and control from University of California, Los Angeles in 2020. He is now directing the Center of Intelligence in the Laboratory of Human-Robot Systems, Peking University. His research interests include perception, control and optimization of robotic systems.

Prof. Han Ouyang received his Ph.D. from the University of Chinese Academy of Sciences in 2019. And his bachelor's degree from Southwest University of Science and Technology in 2014. He joined School of Nanoscience and Engineering of University of the Chinese Academy of Sciences as the Doctoral supervisor, Associate Professor. His research interests focusing on the theories and technologies of self-powered materials and devices with the goal of electrical stimulation disease treatment and diagnosis. He carry out cross-research work on new materials, electrical stimulation medical devices, and disease diagnosis and treatment.

Prof. Zhou Li received his Ph.D. from Peking University in Department of Biomedical Engineering in 2010, and Bachelor's Degree from Wuhan University in 2004. He joined School of Biological Science and Medical Engineering of Beihang University in 2010 as an Associate Professor. Currently, he is a Professor in Beijing Institute of Nanoenergy and Nanosystems, Chinese Academy of Sciences. His research interests include nanogenerators, in vivo energy harvesters, self-powered medical devices, and biosensors.

Prof. Qining Wang received the Ph.D. degree in dynamics and control from Peking University, Beijing, China, in 2009. He is currently a Full Professor with the College of Engineering, Peking University. He is also the Vice-Dean with the College of Engineering, Peking University. His research interests include wearable robotics and human–machine interfaces.